Biomaterials and Biosystems 6 (2022) 100045

Contents lists available at ScienceDirect

Biomaterials and Biosystems

journal homepage: www.elsevier.com/locate/bbiosy

Bioengineered PLEKHA7 nanodelivery regularly induces behavior alteration and growth retardation of acute myeloid leukemia

Sameh A. Mohammed[a,b], Yasuhiro Kimura[a], Yuhki Toku[a], Yang Ju[a,*]

[a] Department of Micro-Nano Mechanical Science and Engineering, Graduate School of Engineering, Nagoya University; Furo-cho, Chikusa-ku, Nagoya, 464-8603, Japan
[b] Department of Pharmacology and Toxicology, Faculty of Pharmacy, Beni-Suef University, Beni-Suef, 62514, Egypt

ARTICLE INFO

Keywords:
Acute myeloid leukemia
PLEKHA7
Nanoparticles
Modulator
Normal homeostasis

ABSTRACT

Acute myeloid leukemia (AML) is the most lethal leukemia with an extremely poor prognosis and high relapse rates. In leukemogenesis, adhesion abnormalities can readily guide an imbalance between hematopoietic progenitor cells and bone marrow stromal cells, altering the normal hematopoietic bone marrow microenvironment into leukemic transformation that enhances leukemic proliferation. Here, we have firstly studied the PLEKHA7 expression in leukemic cells to assess their growth capability affected by the restoration of PLEKHA7 in the cells. The efficacy of PLEKHA7-loaded cRGD-mediated PEGylated cationic lipid nanoparticles for efficient PLEKHA7 delivery in leukemic cells as well as the effect of PLEKHA7 on the regulated induction of AML behavior and growth alterations were investigated. PLEKHA7 re-expression diminished colony-forming ability and reinforced the incidence of growth retardation without apoptosis in AML cell lines. PLEKHA7 regulated the restoration of cell surface adhesion and integrity during normal homeostasis. Our findings revealed that PLEKHA7 functions as a behavior and growth modulator in AML. To our knowledge, the role of PLEKHA7 in AML had not been studied previously and our data could be exploited for further mechanistic studies and insights into altering human AML behavior and growth.

1. Introduction

Acute myeloid leukemia (AML) is an aggressive heterogeneous blood cancer caused by the unusual differentiation and proliferation of marrow cells (myeloid blasts) initiated by the spleen, peripheral blood, and bone marrow. AML is characterized by poor survival rates in older adults and children with multiple genetic mutations and high relapse rates in patients [1, 2]. Hematopoietic homeostasis is maintained via adult normal hematopoiesis, which takes place within the bone marrow microenvironment. The regulation of hematopoietic progenitor differentiation and proliferation in the bone marrow microenvironment could produce an interaction balance between hematopoietic progenitor cells and bone marrow stromal cells [3, 4]. Some molecules can manage stromal cells, such as cell adhesion molecules [5].

PLEKHA7, belonging to the pleckstrin homology domain-containing protein family A, is a protein of adherens junctions (AJs), accommodating to the apical zonula adherens (ZA) in epithelial cells and engaging in a structural complex for junction morphogenesis and stabilization [6]. While E-cadherin-based cell-cell contacts are created across lateral membranes among adjacent cells, mature AJs manifest in well-differentiated epithelial cells and particularly centralize at the apical areas of cell-cell contact, whereby they combine with actin filaments to generate ZA [7, 8]. PLEKHA7 exhibits outstanding mediation of cell-cell adhesion through specific interactions at the AJs of cells. PLEKHA7 plays a fundamental role in epithelial integrity whereby they combine to associate with actin filaments in the cytoskeleton [9, 10]. Consequently, several studies have discussed the dual oncogenic and tumor suppression activities of PLEKHA7 according to cancer type, such as breast cancer [11, 12].

Tumorigenesis has been generated from PLEKHA7 loss, which interferes with the E-cadherin/EGFR signaling pathway, promoting cancer cell growth and progression [13, 14]. Recent studies have reported structural variations between apical AJs and the basolateral areas of cell-cell contact. For instance, the PLEKHA7-binding p120 is mainly located at the apical AJs of well-differentiated epithelial cells, but this PLEKHA7-binding p120 composite is not found in the lateral areas of cell-cell contact [15–17]. Additional reports revealed that basolateral cell-cell complexes without PLEKHA7 could enhance tumorigenesis, while the apical AJs could result in tumor suppression via PLEKHA7 [13, 15, 18]. Furthermore, E-cadherin is widely expressed in areas of cell-cell contact in kidney and breast cancers, whereas PLEKHA7 is still widely downregulated or mislocalized[11,15] at the apical AJs. In leukemogen-

* Corresponding author at: Department of Mechanical Science and Engineering, Graduate School of Engineering, Nagoya University, Furo-cho, Chikusa-ku, Nagoya 464-8603, Japan.
E-mail address: ju@mech.nagoya-u.ac.jp (Y. Ju).

https://doi.org/10.1016/j.bbiosy.2022.100045
Received 18 November 2021; Received in revised form 18 March 2022; Accepted 22 March 2022

esis, adhesion abnormalities can readily induce an imbalance between hematopoietic progenitor cells and bone marrow stromal cells, altering the normal hematopoietic bone marrow microenvironment into a leukemic microenvironment, enhancing leukemic growth and prohibiting leukemic cell apoptosis [19–21]. In this study, we investigated the effect of PLEKHA7 on the dynamics and behavior of AML cells and how the existence of PLEKHA7 modulates AML characterizations to open a different orientation for the alteration of AML cell growth. Since the role of PLEKHA7 in AML has not been studied previously, we attempted to demonstrate the correlation between PLEKHA7 expression and the incidence of AML growth. We delivered PLEKHA7 protein harnessing cRGD-mediated PEGylated cationic lipid nanoparticles to restore adhesion normality and integrity in AML cells, thereby resulting in the regulated induction of AML behavior alteration for normal homeostasis.

Outstandingly, targeted drug delivery systems, such as multifunctional biodegradable lipid nanoparticles, have been engineered to manifest considerable strategies to ameliorate many cargo loading challenges [22–24]. Incorporation of inert polymers such as polyethylene glycol (PEG) robustly reinforces the surface functionalization of cationic nanoliposomal nanostructures to form more sterically stabilized nanoparticles [25–27] and protect them from macrophage capture, aggregation, and reticuloendothelial system clearance, thereby prolonging retention time in the blood stream [28, 29]. For selective targeting, surface ligands such as cyclic arginine-glycine-aspartate (RGD), which combines explicitly with $\alpha v\beta 3$ integrin with high affinity, could promote cell-nanomaterial interactions, allowing cargo penetration into the pathologic location [30–32]. The RGD{d-Phe}{Lys(PEG-Mal)} sequence was synthesized from the chemical linkage of c(RGDfK) with thiolated PEG (NHS-PEG6-maleimide) associated with head-to-tail cyclic modification to acquire a bioengineered surface for optimal functionalization of the fabricated nanostructures.

In our current study, we synthesized cRGD-tagged PEGylated cationic nanoliposomes for PLEKHA7 delivery to regulate the induction of AML behavior and growth alterations to emerge as a potential target for AML modulation (Fig. 1A, B). This research is the first preclinical trial of PLEKHA7-based AML. Lipo-PLEKHA7-PEG-cRGD mainly displayed a significant mitigating effect on cell proliferation and colony formation with noticeable adhesion integrity. Therefore, our findings shed new light on PLEKHA7 as an AML behavior and growth modulator, consistent with the application of bioengineered PLEKHA7 nanoparticles, representing a prospective insight for human AML behavior alteration and modulation.

2. Materials and methods

2.1. Preparation of nanoparticles

The PLEKHA7 stock solution was first prepared at 10 μg/mL and gently mixed with complexation buffer at a 1:1 mol ratio for use as diluted PLEKHA7 (50 μL stock diluted in 100 μL Opti-MEM medium (Gibco) just before use) and with Lipofectamine RNAiMAX reagents/invivofectamine 3.0 (Invitrogen). The complex was incubated for 30 min at 50 °C, sonicated for 1 h, centrifuged at 500 g for 5 min at 25 °C, and washed three times with deionized water to collect PLEKHA7-loaded cationic liposomal nanoparticles (Lipo-PLEKHA7).

For the preparation of PLEKHA7-loaded cRGD-guided PEGylated cationic liposomal nanoparticles (Lipo-PLEKHA7-PEG-cRGD), c(RGDfK) linked with thiolated PEG (NHS-PEG6-maleimide) associated with head to tail cyclic modification for cell surface $\alpha v\beta 3$ receptors targeting to form RGD{d-Phe}{Lys(PEG-Mal)} sequence construct, which was purchased from GenScript (peptide-081,102 ID: J7777DK130), and was then dissolved in PBS solution with pH 7.4 to be stored as a stock. This procedure was repeated without addition of PLEKHA7 protein to fabricate Lipo-PEG-cRGD nanoparticles.

Subsequently, 100 μL of this stock solution was added to the previously prepared lipid nanoparticle-entrapped PLEKHA7. The resultant mixture was continuously stirred for 24 h at 25–30 ºC in the dark. The nanoparticles were finally recovered by centrifugation at 100 g for 10 min at 25 °C and washed three times with deionized water.

Fluorescently labeled Lipo-PLEKHA7-PEG-cRGD nanoparticles were also prepared by the same protocol through conjugation of PLEKHA7 with the red fluorescent dye ATTO 550 (Sigma-Aldrich) solution. Briefly, 50 μL of PLEKHA7 solution was mixed with 30 μL of biologically free water (Invitrogen), 10 μL of binding solution (Thermo Fisher Scientific), and 10 μL of ATTO 550 solution to obtain 100 μL of the final complex.

FITC-labeled Lipo-PLEKHA7-PEG-cRGD nanoparticles were also prepared by the same protocol through conjugation of PLEKHA7 with FITC (Sigma-Aldrich) solution.

2.2. Characterization

The size and zeta potential of Lipo-PLEKHA7-PEG-cRGD nanoparticles was measured by dynamic light scattering using a Malvern Nano ZS90 Zetasizer (Malvern Instruments). Transmission electron microscopy (TEM) was performed using a JEOL 1200 EX transmission electron microscope. The morphologies of PLEKHA7-loaded cRGD-tagged PEGylated cationic nanoliposomes (Lipo-PLEKHA7-PEG-cRGD) characterized by DLS measurements showed optimal physicochemical properties, as evidenced by hydrodynamic diameter and zeta potential values. TEM findings indicated efficient PLEKHA7 encapsulation by the PEGylated modified surface conjugated with the targeted cRGD ligand.

2.3. Cell culture

The current study was performed on two different AML cell lines. Firstly, a human KG-1a cell line (ECACC 91030101) was obtained from Cell Bank, Riken BRC, Japan). The cells were originated from Human Caucasian bone marrow acute myelogenous leukemia as a lymphoblast cell type. KG-1a cell line was derived from the parental KG-1 cells without responsiveness to colony stimulating factor in soft agar culture or to expression to the la-like antigen. The cells were cultured in IMDM (Gibco) supplemented with 20% heat-inactivated fetal bovine serum (FBS, Gibco). Secondly, a human ML-2 cell line (ACC 15) was obtained from DSMZ (Braunschweig, Germany). These cells were originated from the peripheral blood of patient with acute myeloid leukemia (AML M4) at diagnosis of AML (following T-non-Hodgkin lymphoma and T-ALL). These cells were cultured in RPMI-1640 (Gibco) supplemented with 10% heat-inactivated fetal bovine serum (FBS, Gibco). Both types of cells were maintained at 37 °C in a 5% CO_2 atmosphere.

2.4. Delivery study

Plekha7 in the pcDNA3.1-C-(K)DYK ORF clone (OHu22298D) was obtained from GenScript. KG-1a and ML-2 cells were transfected with diluted PLEKHA7, Lipo-PLEKHA7, Lipo-PEG-cRGD and Lipo-PLEKHA7-PEG-cRGD nanoparticles and were investigated to explore PLEKHA7 effectiveness in our experimental design.

2.5. Intracellular uptake and colocalization analysis

KG-1a cells were seeded in 35-mm glass-bottom dishes (Iwaki AGC Techno Glass, Japan) at a density of 4×10^4 cells per well 1 d before transfection. Lipo-PLEKHA7-PEG-cRGD nanoparticles were prepared with ATTO 550 (Sigma-Aldrich) fluorophore (red) to track the intracellular location of the nanoparticles. After 4 h of incubation, cells were fixed with 4% paraformaldehyde in PBS (Sigma-Aldrich) for 15 min and were further stained with Hoechst 33342 (Molecular Probes) and ConcanavalinA-FITC (Sigma-Aldrich) for nuclei (blue) and cell membrane (green) labeling, respectively. The cells were imaged using a TiE-A1R confocal laser scanning microscope (Nikon). 3D images of the cells were obtained using Z-stack mode measurements. Images were analyzed using Nikon imaging software (NIS-Elements Viewer 4.50).

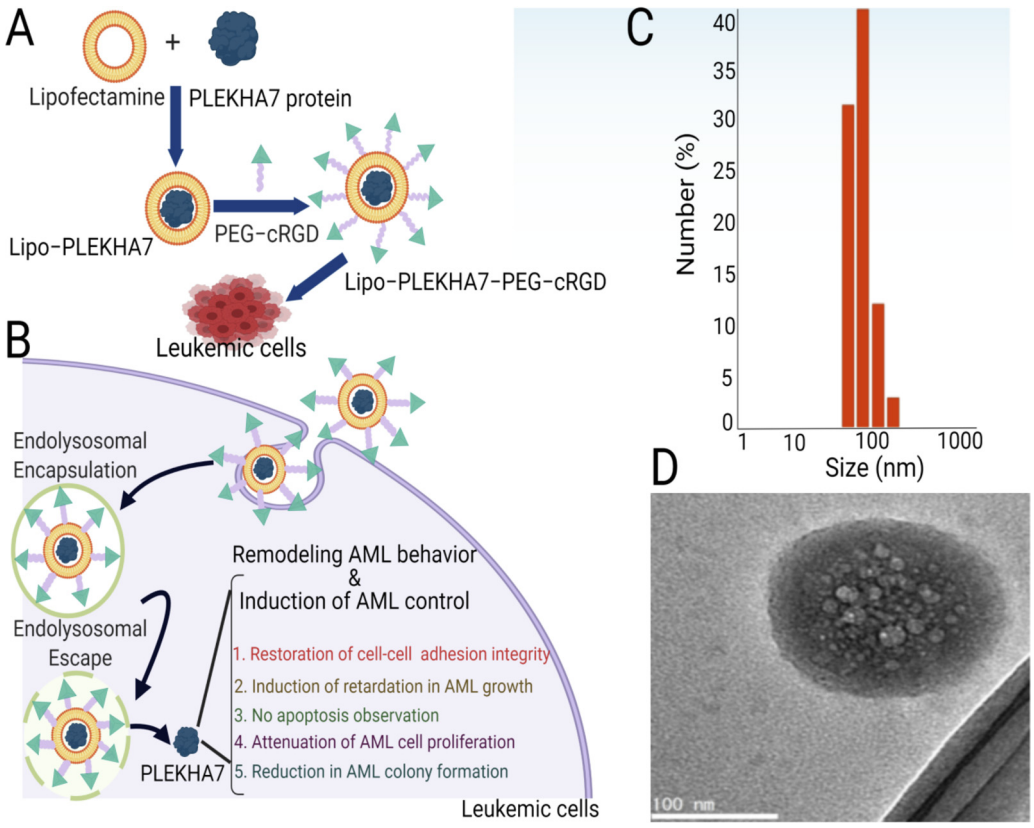

Fig. 1. Synthesis and Characterization of Lipo-PLEKHA7-PEG-cRGD nanoparticles for efficient delivery to leukemic cells. (A) Schematic illustration of synthetic Lipo-PLEKHA7-PEG-cRGD nanoparticles for AML delivery. (B) Proposed mechanism of the cellular uptake of Lipo-PLEKHA7-PEG-cRGD nanoparticles for alterations of AML cell behavior and growth. (C) Dynamic light scattering plot of Lipo-PLEKHA7-PEG-cRGD (n = 3). (D) Transmission electron microscope images of Lipo-PLEKHA7-PEG-cRGD. (scale bar = 100 nm, n = 3).

For flow cytometry analysis, KG-1a cells were seeded in 96-well plates and harvested after 4 h for flow cytometry using FACS CantoII (BD Biosciences, Franklin, NJ, USA).

Visualization of FITC-labeled Lipo-PLEKHA7-PEG-cRGD for colocalization analysis KG-1a cells was seeded in 35-mm glass-bottom dishes (Corning) at a density of 4×10^4 cells per well 1 d before transfection. FITC-labeled Lipo-PLEKHA7-PEG-cRGD nanoparticles were prepared (green) to track the intracellular location of the nanoparticles. After 12 h of incubation, the cells were fixed with 4% paraformaldehyde in PBS (Sigma-Aldrich) for 20 min and then directly stained with phalloidin (red) for F-actin labeling.

2.6. Western blotting

KG-1a cells were treated with Lipo-PLEKHA7-PEG-cRGD for 3 d, and further cultured for 2 d before lysis. The cells were suspended in a radioimmunoprecipitation (RIPA) lysis buffer (Santa Cruz Biotechnology, Dallas, TX, USA) for whole-cell lysis. Proteins were separated by SDS-PAGE and blotted onto the PVD membrane (Millipore). The same protocol was repeated with untreated KG-1a cells as a control cells to investigate PLEKHA7 expression in the cells before and after the addition of Lipo-PLEKHA7-PEG-cRGD. Images were captured, and chemiluminescent signals were analysed using ImageQuant LAS 4010 (GE Healthcare, Chicago, IL, USA). Western blot experiments were performed using the following antibodies: anti-PLEKHA7 (PA585686, 1:1000 working dilution, overnight shaking incubation at 4 °C), Cruz Marker molecular weight standards (sc-2035), β-actin (sc-47,778, 1:5000 working dilution, overnight shaking incubation at 4 °C) from Santa Cruz Biotechnology and secondary horseradish peroxidase (HRP)-conjugated antibody from Abcam (ab205718, 1:2000 working dilution, incubation at 25 °C for 1 h). Image J software was used to quantify PLEKHA7 protein expression in KG-1a cells.

2.7. Proliferation assay and CFC assay

For the proliferation assay, 1×10^4 KG-1a and ML-2 cells were seeded in 96-well plates 1 d before transfection, incubated for 2 d, and determined at day 3 with CellTiter 96 AQueous Non-Radioactive Cell Proliferation Assay (Promega) according to the manufacturer's instructions. Colony formation assay was performed by plating 1000 cells per well of a 6-well plate, transfected, and incubated for 7 d The colonies were fixed with a fixing reagent (methanol:acetic acid, 3:1 v/v) and stained with 0.5% crystal violet in 20% methanol for 15 min.

2.8. Cell apoptosis assay

Cell apoptosis was evaluated using an Annexin V-FITC apoptosis detection kit following the manufacturer's protocol (Thermo Fisher Scientific) and analyzed with a FACS CantoII flow cytometer (BD Biosciences). KG-1a cells were seeded into 35 mm glass-bottom dishes (Corning) and transfected with naked PLEKHA7, Lipo-PLEKHA7, Lipo-PEG-cRGD and Lipo-PLEKHA7-PEG-cRGD nanoparticles for 24 h. After two washes with PBS, the cells were stained with 5 μL Annexin V-FITC and PI, mixed with Annexin V binding buffer (500 μL), and incubated at 25 °C in the dark for 15 min.

2.9. Adhesion-associated proliferation assay

Briefly, 1×10^6 KG-1a cells were seeded in 48-well plate and transfected with naked PLEKHA7, Lipo-PLEKHA7, Lipo-PEG-cRGD and Lipo-PLEKHA7-PEG-cRGD nanoparticles for 2 d After washing, KG-1a cells

were resuspended in a Collagen |-coated 48-well plate and were incubated at 37 ˚C for 20 min to allow the cells to adhere with the surface. To washing off the non-adherent cells, 200 µl IMDM were added to each well to wash and repeated 4 times. After complete washing, cells were recovered by adding fresh media and were incubated at 37 ˚C for 4 h. CellTiter 96 AQueous Non-Radioactive Cell Proliferation Assay (1 mg/ml) was added to each well and cells were continuously incubated at 37 ˚C for 2 h. The cell count of the adhered cells was assayed by the measurement of absorbance signals to evaluate the surface adhesion capability of the cells.

2.10. Fluorescence and cell surface adhesion studies

For cell surface adhesion investigation, KG-1a cells were seeded into 35 mm glass-bottom dishes (Corning). Untreated cells, naked PLEKHA7 treated cells and Lipo-PEG-cRGD treated cells were used for the comparison with the cells treated with Lipo-PLEKHA7-PEG-cRGD by utilizing the following stains; FITC (green) for cell membrane, ATTO 550 (red) for actin and Hoechst 33,342 (blue) for nuclei. KG-1a cells were treated with FITC-labeled Lipo-PLEKHA7-PEG-cRGD nanoparticles for 24 h. After washing twice with PBS, the cells were counterstained with 4,6-Diamidino-2-phenylindole (DAPI; D1306, Invitrogen) for nuclei staining and then visualized using an inverted fluorescence microscope (Keyence BZ-9000, Osaka, Japan).

For monitoring the restoration of cell surface adhesion induced by PLEKHA7, KG-1a cells were seeded in 35-mm glass-bottom dishes (Iwaki AGC Techno Glass, Japan) at a density of 1×10^5 cells per well 1 d before transfection. ATTO 550- labeled Lipo-PLEKHA7-PEG-cRGD nanoparticles were used for cell transfection for 12 h. The cells were fixed with 4% paraformaldehyde in PBS (Sigma-Aldrich) for 15 min and were further stained with Hoechst 33342 (Molecular Probes) and ConcanavalinA-FITC (Sigma-Aldrich) for nuclei (blue) and cell membrane (green) labeling, respectively. The cells were imaged using a TiE-A1R confocal laser scanning microscope (Nikon).

In order to further confirm cell surface adhesion, cells treated with Lipo-PLEKHA7-PEG-cRGD nanoparticles were compared with untreated cells, for which KG-1a cells were seeded into 96-well plates (at a density of $\sim 4 \times 10^4$ cells/well), incubated for 4 h, and then treated with Lipo-PLEKHA7-PEG-cRGD. After washing twice with PBS, the cells were stained with IncuCyte NucLight Rapid Red Reagent for nuclear labeling (Essen Bioscience) and the images were captured at 1 h scan intervals for 24 h.

2.11. Live cell imaging and cell growth assay

For live cell imaging, cells treated with Lipo-PLEKHA7-PEG-cRGD nanoparticles were compared with untreated cells. KG-1a cells were seeded into 96-well plates (at a density of $\sim 4 \times 10^4$ cells/well), incubated for 4 h, and then treated with Lipo-PLEKHA7-PEG-cRGD. After washing twice with PBS, the cells were suspended in fresh media and were monitored in the IncuCyte ZOOM (Essen BioScience), acquiring images at 1 h scan intervals for 48 h.

For cell growth assessment, KG-1a and ML-2 cells were seeded into 96-well plates (at a density of $\sim 4 \times 10^4$ cells/well), incubated for 4 h, and then treated with Lipo-PLEKHA7-PEG-cRGD. After washing twice with PBS, the cells were stained with IncuCyte NucLight Rapid Red Reagent for nuclear labeling (Essen Bioscience) and were monitored in the IncuCyte ZOOM (Essen BioScience), acquiring images at 1 h scan intervals for 48 h.

For cell growth quantification, transfected cells and untreated cells were seeded in 96-well plates (5000 cells/well) using IncuCyte ZOOM (Essen Bioscience) for every 1 h of imaging. The confluence was analyzed using the IncuCyte ZOOM 2016A software.

2.12. Statistical analysis

Statistical significance was analyzed by Student's *t*-test and ANOVA using JMP Pro 15 software (SAS Institute Inc., Cary, NY, USA), and the data are presented as the mean ± SEM, $^{*}p < 0.05$; $^{**}p < 0.01$; $^{***}p < 0.001$.

3. Results

3.1. Nanoparticles synthesis and characterization

To provide a biodegradable nanoplatform for PLEKHA7 delivery to AML cells, cRGD-guided PEGylated cationic lipid nanoparticles were prepared. Nanoparticles were conjugated with cyclic RGD peptide as a surface ligand for $\alpha_v\beta_3$ integrin targeting to avoid the PEG dilemma and expedite targeted, efficient delivery. The particle size and zeta potential values are listed in Table S1. The average diameter of Lipo-PLEKHA7-PEG-cRGD was 172.3 ± 12.1 nm, while the zeta potential was 29.22 ± 1.3 mV (Fig. 1C and Fig. S1, respectively). The resultant polydispersity index indicated that the synthesized nanoparticles were stable in water with a narrow size dispersion. As shown in the TEM images (Fig. 1D), the prepared nanoparticles were spherical and manifested a proper structure and configuration. The morphology of Lipo-PLEKHA7-PEG-cRGD revealed a uniform spherical shape and narrow size distribution.

3.2. Intracellular uptake of Lipo-PLEKHA7-PEG-crgd nanoparticles

Effective intracellular uptake of synthetic nanoparticles is a fundamental necessity for evidence of therapeutic efficiency. Lipo-PLEKHA7-PEG-cRGD uptake by KG-1a cells was examined by confocal microscopy (Fig. 2A). KG-1a cells were successfully transfected with ATTO 550 red-labeled Lipo-PLEKHA7-PEG-cRGD, accompanied by the observation of Lipo-PLEKHA7-PEG-cRGD located in the cytoplasm after 4 h of incubation. As demonstrated in the merged image for investigating the comprehensive cellular uptake, the aggregated dots of ATTO 550 red-labeled Lipo-PLEKHA7-PEG-cRGD were largely displayed in the cytoplasm. Moreover, 3D images in Fig. 2B revealed a considerable boost of ATTO 550 red-labeled Lipo-PLEKHA7-PEG-cRGD; thus, these findings also confirmed higher intracellular uptake efficiency of Lipo-PLEKHA7-PEG-cRGD inside KG-1a cells (Fig. 2C). Our results showed that Lipo-PLEKHA7-PEG-cRGD undergoes $\alpha_v\beta_3$ receptor-mediated endocytosis.

3.3. Lipo-PLEKHA7-PEG-cRGD exhibits efficient transfection and distribution into KG-1a cells

The performance of colocalization analysis was indispensably required to emphasize high transfection and distribution of Lipo-PLEKHA7-PEG-cRGD nanoparticles inside KG-1a cells after 12 h incubation. As shown in Fig. 2D, the visible colocalization between FITC-labeled Lipo-PLEKHA7-PEG-cRGD (green) and phalloidin-labeled actin filaments (red) was exhibited for the regulated distribution of PLEKHA7 at the apical ZA location, indicating effective transfection of the fabricated nanoparticles for efficient PLEKHA7 delivery.

Altogether, the results of cellular uptake study (Sections 2.3, 3.3) highlight that PLEKHA7 was encapsulated in the nanoparticles without bulky aggregation or degradation.

3.4. Lipo-PLEKHA7-PEG-cRGD induces PLEKHA7 re-expression in KG-1a cells

To elucidate PLEKHA7 expression in KG-1a cells before and after transfection with Lipo-PLEKHA7-PEG-cRGD nanoparticles, immunoblotting experiment was performed to assess the comparison between KG-1a untreated cells with cells treated with Lipo-PLEKHA7-PEG-cRGD nanoparticles. The results confirmed our claim displaying that

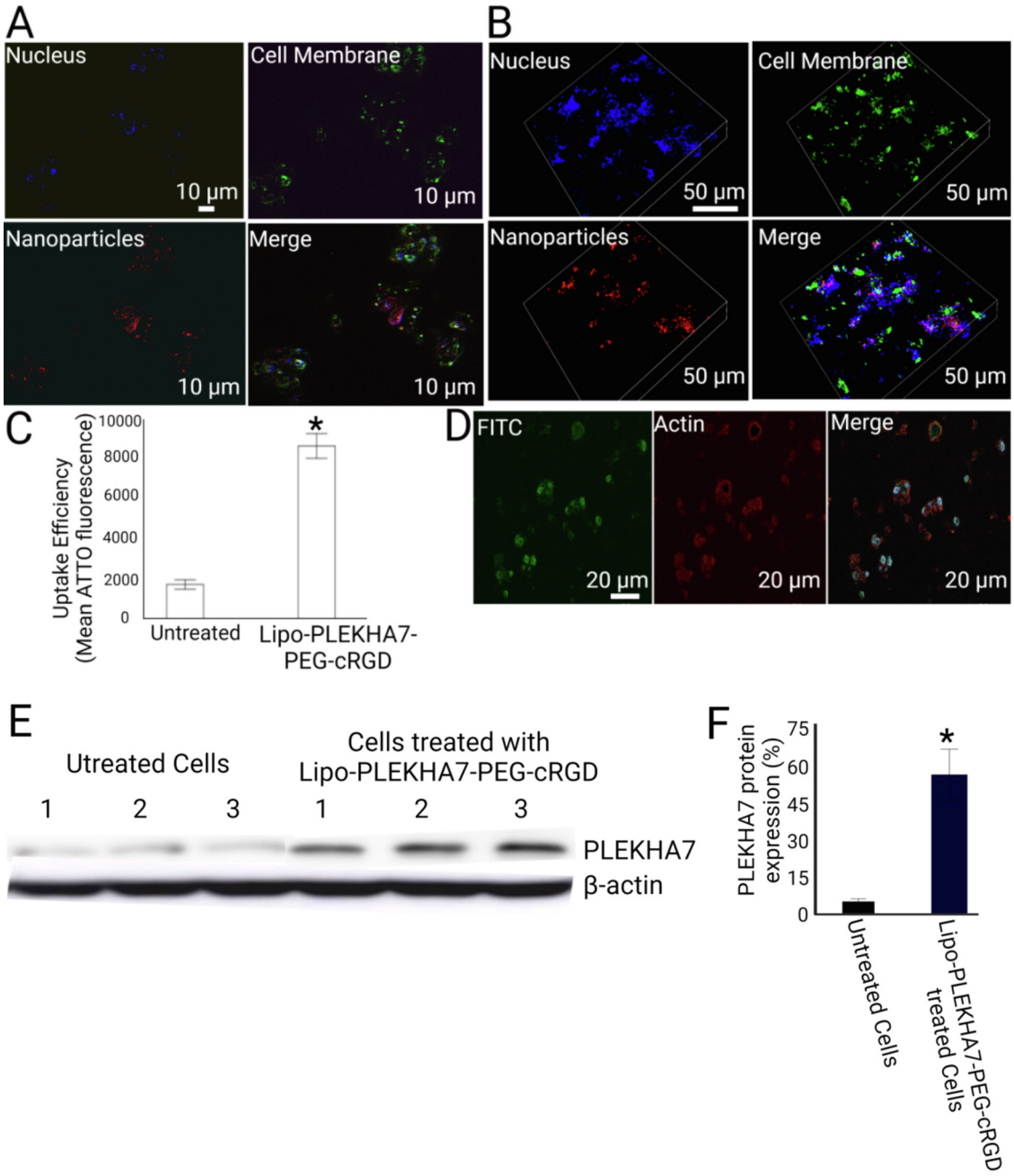

Fig. 2. Cellular uptake of Lipo-PLEKHA7-PEG-cRGD nanoparticles in KG-1a cells. (A) Uptake of fluorescently labeled Lipo-PLEKHA7-PEG-cRGD into KG-1a cells. Scale bar = 10 µm. (B) 3D cellular uptake snapshots of fluorescently labeled Lipo-PLEKHA7-PEG-cRGD into KG-1a cells. Scale bar = 50 µm. The color representatives are blue (Hoechst 33,342) for nuclei, green (Concanavalin A-FITC) for cell membrane, and red (ATTO 550) for Lipo-PLEKHA7-PEG-cRGD nanoparticles. (C) Cellular uptake efficiency of Lipo-PLEKHA7-PEG-cRGD in KG-1a cells. Data are presented as mean ± SEM (n = 3 biological replicates). Statistical significance was set at $^{*}p < 0.05$. (D) Colocalization study of FITC-labeled Lipo-PLEKHA7-PEG-cRGD nanoparticles for efficient transfection in leukemic cells. Fluorescently labeled Lipo-PLEKHA7-PEG-cRGD were monitored in KG-1a cells. The color representatives are green (FITC) for PLEKHA7 and red (phalloidin) for actin. Scale bar = 20 µm. (E) Western blots showing PLEKHA7 protein expression in KG-1a cells prior to and after transfection with Lipo-PLEKHA7-PEG-cRGD compared to untreated cells (n = 3). (F) Quantification of PLEKHA7 protein expression in KG-1a cells. Data are presented as mean ± SEM (n = 3 biological replicates); $^{*}p < 0.05$.

PLEKHA7 was lost (in lower expression level) or mis-localized in KG-1a cells while after the addition of nanoparticle-mediated PLEKHA7 delivery, it significantly resulted in PLEKHA7 re-expression inside the cells. As demonstrated in (Fig. 2E, F), PLEKHA7 protein expression was significantly upregulated and re-stored in cells treated with Lipo-PLEKHA7-PEG-cRGD with approximately 50% PLEKHA7 protein expression increase in comparison with untreated cells at $p < 0.05$.

3.5. Lipo-PLEKHA7-PEG-cRGD attenuates cell proliferation and clonogenic growth of AML cells

As demonstrated in Fig. 3A and B, cell counting revealed that Lipo-PLEKHA7-PEG-cRGD nanoparticles considerably reduced the proliferation rate in KG-1a and ML-2 cells compared to control cells. We observed a significant alleviation of AML cell proliferation caused by Lipo-

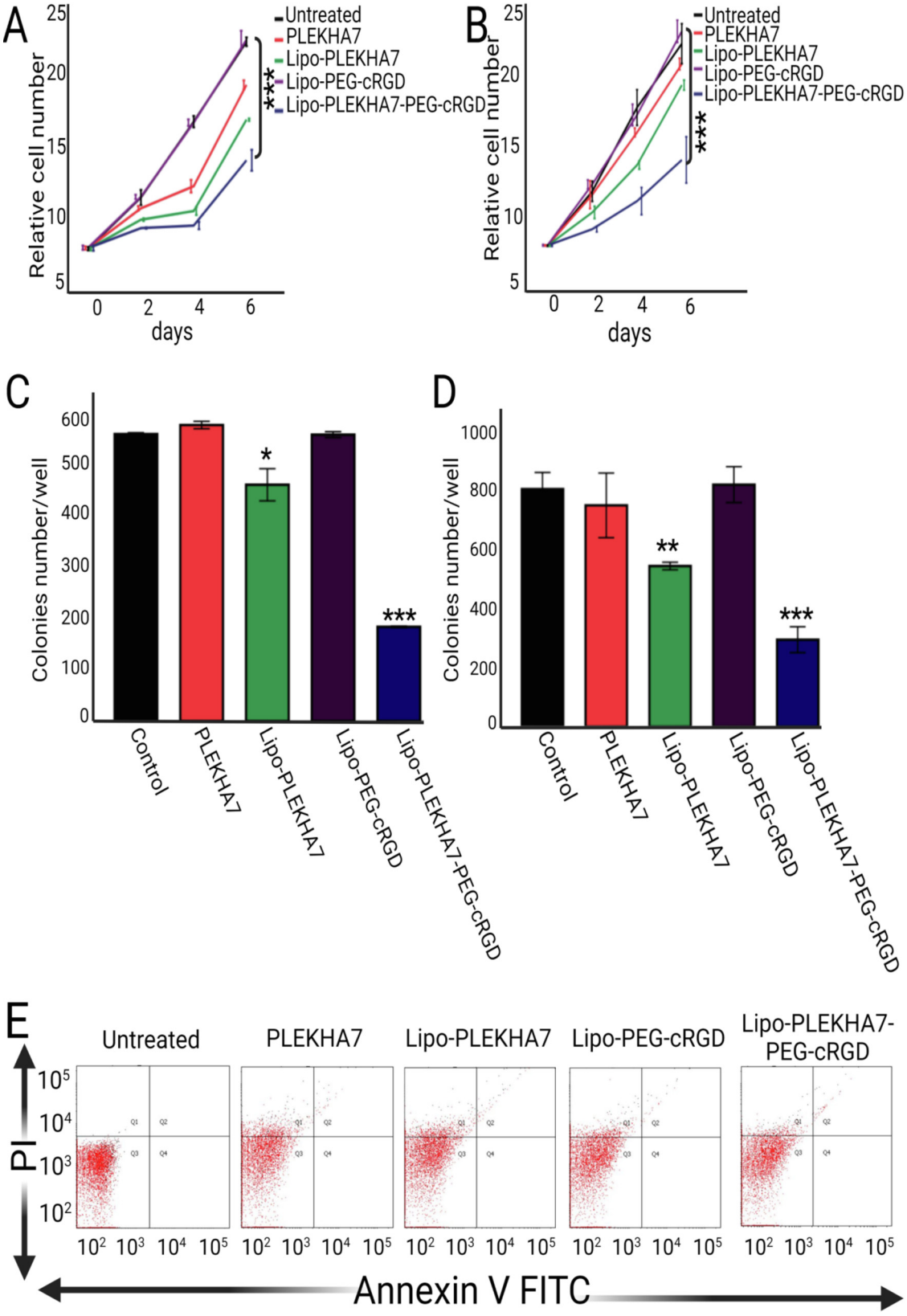

Fig. 3. Proliferation activity of Lipo-PLEKHA7-PEG-cRG nanoparticles on AML cells. (A) Cell count of KG-1a cells and (B) Cell count of ML-2 cells transfected with naked PLEKHA7, Lipo-PLEKHA7, Lipo-PEG-cRGD and Lipo-PLEKHA7-PEG-cRGD nanoparticles in culture comparable to untreated cells. The value is determined as the fold increase in cell number relative to the number of cells initially plated. Data are presented as mean ± SEM ($n = 5$) at $^{***}p < 0.01$. (C) Clonogenic growth of KG-1a cells and (D) Clonogenic growth of ML-2 cells transfected with naked PLEKHA7, Lipo-PLEKHA7, Lipo-PEG-cRGD and Lipo-PLEKHA7-PEG-cRGD nanoparticles relative to untreated cells. The number of colonies observed 7 d after plating. Data are presented as mean ± SEM ($n = 5$); $^{*}p < 0.05$, $^{**}p < 0.01$, $^{***}p < 0.001$. (E) Effect of naked PLEKHA7, Lipo-PLEKHA7, Lipo-PEG-cRGD and Lipo-PLEKHA7-PEG-cRGD nanoparticles on AML cell apoptosis. Representative flow cytometry plot of KG-1a transfected with naked PLEKHA7, Lipo-PLEKHA7, Lipo-PEG-cRGD and Lipo-PLEKHA7-PEG-cRGD nanoparticles relative to untreated cells for Annexin V and PI.

PLEKHA7-PEG-cRGD compared with naked PLEKHA7, Lipo-PLEKHA7 and Lipo-PEG-cRGD. We also noticed that the relative number of colonies formed by naked PLEKHA7, Lipo-PLEKHA7, Lipo-PEG-cRGD and Lipo-PLEKHA7-PEG-cRGD were 592 ± 15, 455 ± 16, 593 ± 13 and 189 ± 11, respectively in KG-1a cells (Fig. 3C) while 786 ± 11, 532 ± 15, 843 ± 10 and 309 ± 12, respectively in ML-2 cells (Fig. 3D). Lipo-PLEKHA7-PEG-cRGD nanoparticles were correlated with the lowest average colony numbers, roughly 70% reduction in both leukemic cell lines compared to control cells ($p < 0.001$). Our findings indicate that Lipo-PLEKHA7-PEG-cRGD markedly attenuated cell proliferation, as evidenced by a dense decline in clonogenic growth of KG-1a and ML-2 cells.

3.6. Lipo-PLEKHA-PEG-cRGD effectiveness on AML cells apoptosis

After demonstrating the proliferation-inhibiting function of Lipo-PLEKHA7-PEG-cRGD nanoparticles on AML cells, the effectiveness of naked PLEKHA7, Lipo-PLEKHA7, Lipo-PEG-cRGD and Lipo-PLEKHA7-PEG-cRGD nanoparticles on cell apoptosis was also investigated. Flow cytometric analysis with Annexin V-FITC/PI double staining was used to evaluate transfected KG-1a cells (Fig. 3E). There was no induction of cell apoptosis when KG-1a cells were transfected with naked PLEKHA7, Lipo-PLEKHA7, Lipo-PEG-cRGD or Lipo-PLEKHA7-PEG-cRGD nanoparticles, showing no significant difference compared to untreated cells. Interestingly, the cell apoptosis study results illustrated that Lipo-PLEKHA7-PEG-cRGD possesses a different direction, completely different from conventional chemotherapeutics.

3.7. Lipo-PLEKHA7-PEG-cRGD maintains ZA integrity in AML cells

We investigated the significant roles of PLEKHA7 in KG-1a cells transfected with Lipo-PLEKHA7-PEG-cRGD nanoparticles, compared to untreated cells and cells transfected with naked PLEKHA7 and Lipo-PEG-cRGD, by inducing the enhancement of surface adhesion of PLEKHA7-mediated cells. As shown in Fig. 4A-E, our results revealed that PLEKHA7 re-expression could restore cell surface morphologic changes associated with surface adhesion in KG-1a cells particularly in Lipo-PLEKHA7-PEG-cRGD group. However, there is no a significant change in untreated cells, naked PLEKHA7 and Lipo-PEG-cRGD groups. To monitor PLEKHA7 location within KG-1a cells, FITC-labeled Lipo-PLEKHA7-PEG-cRGD nanoparticles were selectively located at the ZA along with the nucleus as shown in Fig. 4D. PLEKHA7 was recruited to the cell-cell contact locations in the ZA to regulate ZA integrity, which was lost in AML cells. Where, the superimposed ovals indicate the cell-cell surface adhesion which is created with the contacting of KG-1a cells after PLEKHA7 restoration in its intracellular location. Moreover, ATTO-550 labeled Lipo-PLEKHA7-PEG-cRGD nanoparticles were also delivered and monitored as demonstrated in Fig. 4E, the red dots (PLEKHA7) were efficiently delivered and transfected to distribute inside KG-1a cells. The PLEKHA7 effect was observed that is the induction of cell to cell surface contact and adhesion through the morphological changes associated with adhesion to attach together and to restore the normal cell behavior. This effect took place once PLEKHA7 had been re-expressed within leukemic cells. These results were also emphasized by the quantification of cellular adhesion as revealed in Fig. 4F. KG-1a cells transfected with Lipo-PLEKHA7 and Lipo-PLEKHA7-PEG-cRGD nanoparticles exhibited a significant enhancement in the percentage of cellular adhesion which was measured as mentioned in Section 2.9., approximately 55% and 75% higher than that in control cells ($p < 0.001$). Contrarily, there is no significant change in naked PLEKHA7 and Lipo-PEG-cRGD groups compared to untreated cells. These results were also confirmed by red fluorescence images in Fig. 4G for revealing the cell-cell surface adhesion of cells transfected with Lipo-PLEKHA7-PEG-cRGD nanoparticles. The arrows indicated that the two adjacent cells treated with Lipo-PLEKHA7-PEG-cRGD nanoparticles were attached together to contact each other after 12 and 24 h. While there is no significant change in untreated cells. Intriguingly, restabilization of PLEKHA7 in AML cells could restore the capability cell-cell adhesion, corroborating our PLEKHA7 nanoconstruct concept for acquiring some characteristic features of healthy normal cells to curb the aggressive behavior of AML cells in growth.

3.8. Lipo-PLEKHA7-PEG-cRGD induces growth retardation in AML cells

The presence of PLEKHA7 plays a pivotal role in AML cell growth. During the IncuCyte schedule scans, we revealed noticeable growth retardation of Lipo-PLEKHA7-PEG-cRGD-treated cells compared to untreated cells, as displayed in Fig. 5A and B which were mainly emphasized by the cell growth curve in Fig. 5C. The cell proliferation rate was strikingly attenuated upon transfection with Lipo-PLEKHA7-PEG-cRGD nanoparticles. These findings were supported by Fig. 5D which showed a significant attenuation in cell growth in cells transfected with Lipo-PLEKHA7-PEG-cRGD nanoparticles when compared with untreated cells, highlighting the controllable effect of Lipo-PLEKHA7-PEG-cRGD on ML-2 cell growth. Ultimately, the restoration of PLEKHA7 could re-establish the growth retardation in AML cells to curb the AML aggressiveness.

4. Discussion

PLEKHA7, one of the most important molecules involved in tissue morphogenesis and maintenance of tissue integrity, also functions as a tumor suppressor protein [8, 33]. Numerous studies have reported a strong correlation between PLEKHA7 loss and the initiation of tumors [12, 13, 18, 34]. We have firstly studied the PLEKHA7 expression in leukemic cells to assess the growth capability of leukemic cells under the condition of loss or mis-localization of PLEKHA7, and estimated the efficacy of PLEKHA7-loaded cRGD-mediated PEGylated cationic lipid nanoparticles for efficient PLEKHA7 delivery in leukemic cells as well as the effect of PLEKHA7 on the regulated induction of AML behavior and growth alterations. To further investigate the significance of PLEKHA7 protein in leukemia, we treated leukemia cells with PLEKHA7-loaded cRGD-mediated PEGylated cationic lipid nanoparticles to restore PLEKHA7 expression and examined its effects on PLEKHA7-mediated cellular adhesion and proliferation. The restoration of adhesion normality and integrity, which was lost in AML cells, could result in normal homeostasis through regulated induction of AML behavior and growth alterations.

Specifically, we tested PLEKHA7 expression in AML cells prior to the transfection to understand the importance of PLEKHA7 loss or mis-localization for survival and aggressiveness of AML cells and we also demonstrated that the restoration of PLEKHA7 strengthens apical ZA and restrains AML growth. The results of the current study illustrated that AML cells could be efficiently transfected with Lipo-PLEKHA7-PEG-cRGD nanoparticles, suggesting their internalization assimilation to alter AML behavior and dynamics to control growth.

Notably, lipid bilayer fusion, endocytosis, drug conjugation, and facilitated diffusion of lipofectamine-based formulation [35] with further surface modification by PEGylation allowed the targeting of the $\alpha_v\beta_3$ integrin ligand [36]. These mechanisms demonstrated that Lipo-PLEKHA7-PEG-cRGD could facilitate the entry of the cargo by liposomes (lipid-based nanocarriers) and cRGD peptide which promotes cell-nanomaterial conjugations to allow cargo penetration into the pathologic location to supply optimum delivery of PLEKHA7 for AML normal homeostasis. These important functions of these biocompatible materials have clearly appeared in cell proliferation, colony formation, and adhesion results. Lipo-PLEKHA7 and Lipo-PLEKHA7-PEG-cRGD nanoparticles have significant effects on AML cells when compared to untreated and other groups. Consistent with the hypothesis that PLEKHA7 acts as an adhesion relative modulator, its re-expression in KG-1a and ML-2 cell lines significantly attenuated the cell growth rate. The cell proliferation results of Lipo-PLEKHA7-PEG-cRGD nanoparticles demonstrated

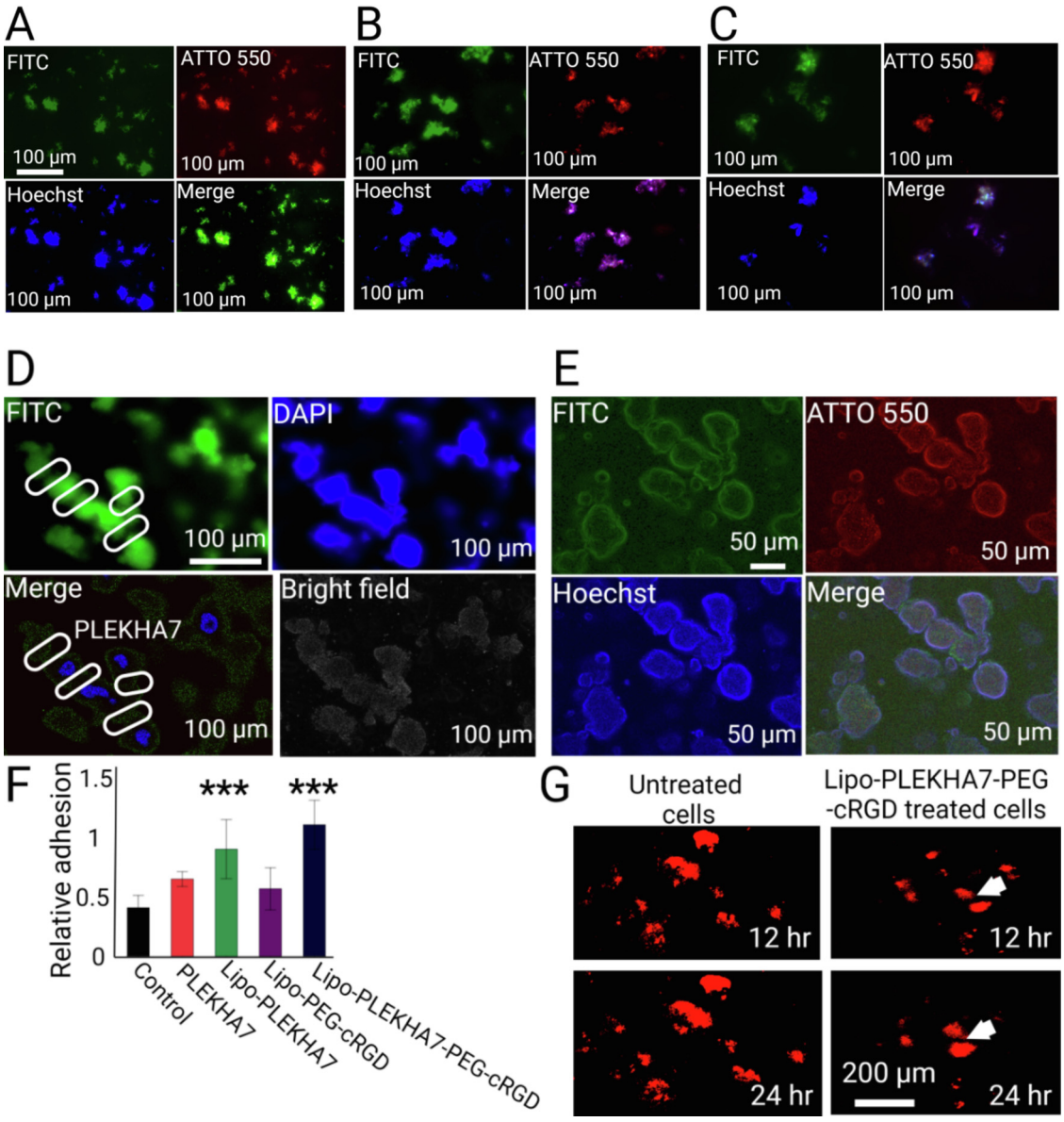

Fig. 4. Effect of Lipo-PLEKHA7-PEG-cRGD nanoparticles on the restoration of normal cell functions. Morphologic appearances associated with adhesion in (A) untreated cells (B) Naked PLEKHA7 treated cells (C) Lipo-PEG-cRGD treated cells. The stain color representatives are green (FITC) for cell membrane, red (ATTO 550) for actin and blue (Hoechst 33,342) for nuclei. Scale bar = 100 µm. (D) Effect of Lipo-PLEKHA7-PEG-cRGD nanoparticles on the restoration of normal cell functions with observation of the exact location of PLEKHA7 within KG-1a cells. Restoration of cell surface adhesion in KG-1a cells transfected with FITC-labeled Lipo-PLEKHA7-PEG-cRGD nanoparticles. The color representatives are green (FITC) for PLEKHA7 and blue (DAPI) for nuclei. Scale bar = 100 µm. (E) Restoration of cell surface adhesion in KG-1a cells transfected with ATTO 550- labeled Lipo-PLEKHA7-PEG-cRGD nanoparticles. The color representatives are blue (Hoechst 33,342) for nuclei, green (Concanavalin A-FITC) for cell membrane, and red (ATTO 550) for Lipo-PLEKHA7-PEG-cRGD nanoparticles. Scale bar = 10 µm. (F) Enhancement effects of PLEKHA7, Lipo-PLEKHA7, Lipo-PEG-cRGD and Lipo-PLEKHA7-PEG-cRGD on the cell adhesion of KG-1a cells in comparison with untreated control. Data are expressed as mean ± SEM (n = 3 biological replicates). Statistical significance was set at $^{***}p < 0.001$. (G) Red fluorescence imaging of KG-1a cells transfected with Lipo-PLEKHA7-PEG-cRGD nanoparticles compared with untreated cells after 12 and 24 h intervals using IncuCyte NucLight Rapid Red Reagent for nuclear labeling showing cell to cell surface adhesion. (Scale bar = 200 µm).

a considerable decrease in cell counting or colony-forming ability, thus displaying high transfection efficiency of nanoparticles in particularly liposomes and cRGD moiety. Lipo-PLEKHA7-PEG-cRGD showed the highest reduction in viable cells (approximately half of total cell numbers) and the lowest clonogenic growth relative to untreated and other indicated groups., promoting efficient PLEKHA7 nanodelivery. The materials utilized in Lipo-PLEKHA7-PEG-cRGD nanostructure for PLEKHA7 delivery have contributed as a biodegradable non-viral vector to efficiently deliver PLEKHA7 cargo to cancer cells without the appearance of therapeutic activity of these biomaterials inside the cells that may cause interference with PLEKHA7 effects. This was evidenced by the results of Lipo-PEG-cRGD in cell proliferation, colony formation and apoptosis experiments. However, it may still have a possibility that the effects of PLEKHA7 protein could be affected by the simultaneous integrin stimulation caused by the nanoparticles. We have observed the appearance of cell to cell adhesion in AML cells after transfection with Lipo-PLEKHA7-PEG-cRGD nanoparticles compared to untreated, naked PLEKHA7 and Lipo-PEG-cRGD groups. These morphological changes in the cells may be related to PLEKHA7 re-expression because it is an apical AJ-specific conjugating partner of p120 catenin to form a regulatory complex which responsible for stabilization of cell to cell surface adhesion and interactions [15,16]. Cell adhesion is a regulatory pro-

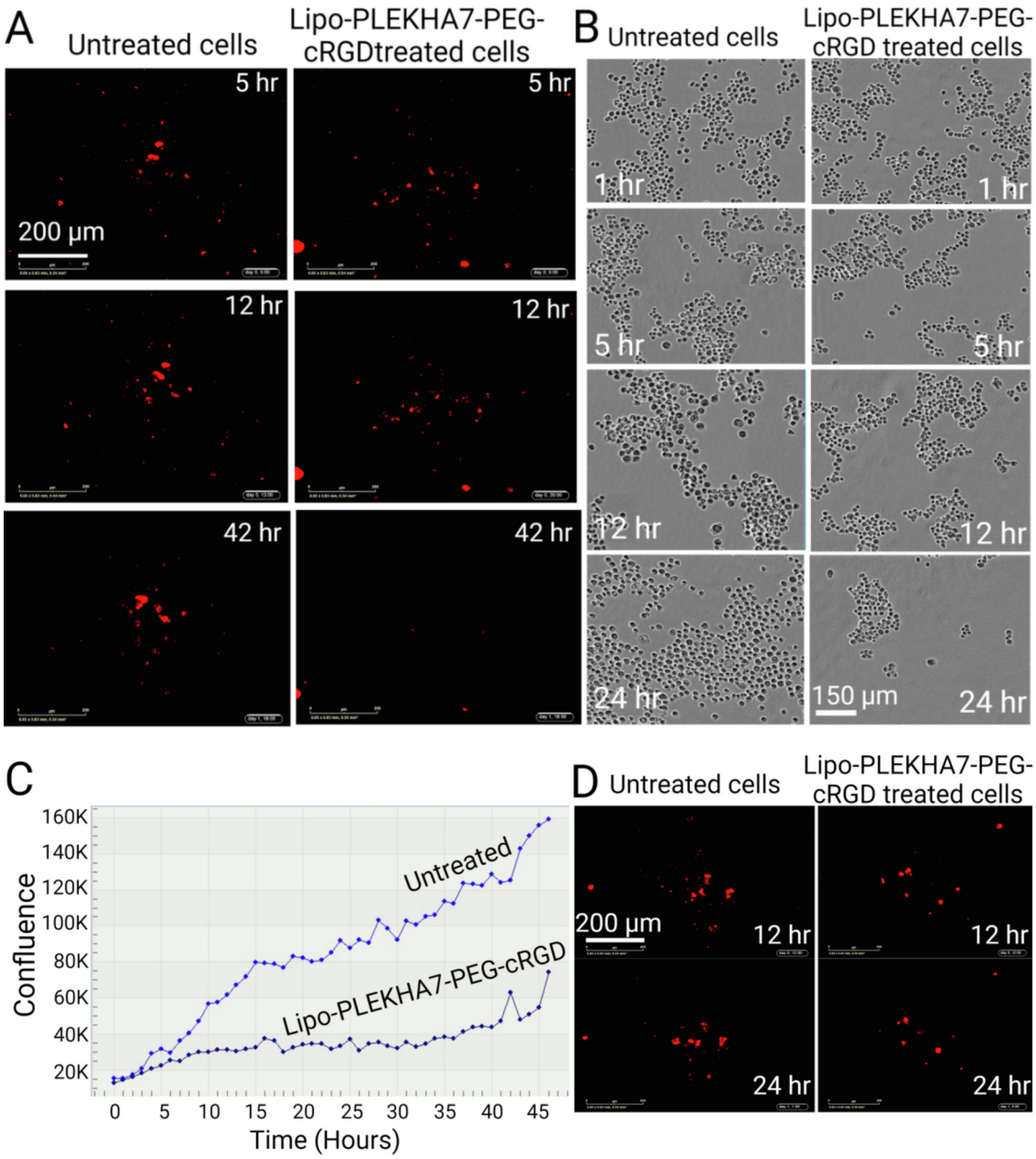

Fig. 5. Growth retardation monitoring of KG-1a cells transfected with Lipo-PLEKHA7-PEG-cRGD nanoparticles. (A) Red fluorescence imaging of KG-1a cells transfected with Lipo-PLEKHA7-PEG-cRGD nanoparticles compared to untreated cells after 5, 12 and 42 h intervals using IncuCyte NucLight Rapid Red Reagent for nuclear labeling showing cell growth retardation. (Scale bar = 200 µm). (B) Live imaging (phase contrast) of KG-1a cells transfected with Lipo-PLEKHA7-PEG-cRGD nanoparticles relative to untreated cells after 1, 5, 12, 24 h intervals demonstrating the induction of AML growth attenuation. (Scale bar = 150 µm). (C) Overall growth over time in KG-1a after transfection with Lipo-PLEKHA7-PEG-cRGD nanoparticles compared with untreated cells. Experiments were performed in triplicate. (D) Red fluorescence imaging of ML-2 cells transfected with Lipo-PLEKHA7-PEG-cRGD nanoparticles compared to untreated cells after 12 and 24 h intervals using IncuCyte NucLight Rapid Red Reagent for nuclear labeling showing growth retardation of the cells (Scale bar = 200 µm).

cess of cell to establish interactions with the neighboring cells through specific protein complexes which could be mediated by adherent junctions [15]. PLEKHA7 is one of these regulatory proteins that directly contributes in the cell to cell adhesion function via p120-specific interacting complex, thus its loss can cause disturbance in cellular interaction and adhesion [16,17]. Moreover, a recent study have reported that PLEKHA7 expression in breast cancer can induces E-cadherin and p120 upregulations which could promote cell to cell adhesion and also inhibit the cancer cell proliferation [12]. We did not investigate the causative mechanism by which PLEKHA7 achieves these behaviors and growth modulator roles in AML. However, previous studies have shown that PLEKHA7 employs the RNAi machinery to the apical AJs to stimulate miRNA maturation and conjugation with an apically localized RNA-induced silencing complex (RISC) [15,34]. This PLEKHA7 role inhibited the expression of pro-tumor-promoting proteins such as cyclin D1, Snail, and c-Myc [15]. A recent study reported concomitant dysfunction of PLEKHA7 and the RNAi machinery at the apical AJs in colon cancer patient samples. Moreover, the RNAi machinery was restored to apical AJs, and PLEKHA7-expressing xenografts showed a reduced tumor burden once PLEKHA7 was restored in colon cancer cell lines [37]. Inhibition of E-cadherin/epidermal growth factor receptor (EGFR) signaling and p120 signaling are the contributing mechanisms that indicate the fundamental role of PLEKHA7 in tumor suppression [13]. In ovarian epithelial cancer, E-cadherin induces EGFR signaling, which is inhib-

ited by PLEKHA7 expression [13]. In AML cells, E-cadherin suppression significantly reduced cell-cell adhesion and enhanced cell growth and colony formation, indicating the function of E-cadherin in homophilic adhesion stimulation and cell proliferation retardation by an E-cadherin-mediated connection with stromal cells [38]. Furthermore, E-cadherin could also suppress the Wnt signaling pathway via β-catenin interaction from the nuclear signaling pool, contributing to its tumor suppression function [39–41]. Prior studies have reported that cell adhesion plays a main role in the interaction between developing hematopoietic cells and their microenvironment, which regulates the destiny of hematopoietic stem cells [42–45]. Zhou et al. demonstrated that the adhesion capacity to bone marrow stroma was impaired in leukemia cells. Hence, the modulation of the adhesion behavior of hematopoietic stem cells may change the hematopoietic cell homeostasis with the bone marrow microenvironment, leading to leukemic transformation [46]. Our results have been agreed with Pence and coauthors that discussed the induction of cancer cells for PLEKHA7 loss or cytoplasmic translocation in order to avoid PLEKHA7 tumor suppression thereby, this suppression caused an extensive burden on cancer cells to eradicate the expression of apical PLEKHA7 [12].

5. Conclusion

Our findings uncovered the important function of PLEKHA7 as a behavior and growth modulator in AML via an in vitro study on new bioengineered smart nanoparticles that are well-characterized, cRGD-conjugated with thiolated PEG (NHS-PEG6-maleimide) to effectively deliver PLEKHA7 to induce normal homeostasis in AML cells. Our study revealed that PLEKHA7 re-expression restores apical ZA integrity and cellular adhesion and attenuates AML growth rate without appearance of apoptosis signals occurred to AML cells. Altogether, This approach will foreseeably open new avenues for applying smart biocompatible PLEKHA7 re-engineered nanoconstructs in vivo via implementation of experimental animal models and further passing into clinical trials for efficient translation and production of advanced PLEKHA7 nanomedicines for AML regulation and reprogramming.

Data statement

All data related to this study can be obtained from the authors on reasonable request.

Declarations of interest

All authors declare that there is no conflict of interest.

CRediT authorship contribution statement

Sameh A. Mohammed: Conceptualization, Methodology, Formal analysis, Visualization, Writing – original draft. **Yasuhiro Kimura:** Data curation, Validation. **Yuhki Toku:** Data curation, Validation. **Yang Ju:** Conceptualization, Investigation, Funding acquisition, Supervision, Writing – review & editing.

Acknowledgments

This work was supported by the Japan Society for the Promotion of Science under Grants-in-Aid for Scientific Research (grant number: 17H06146). We thank Yorifuji Eri for excellent technical assistance and training courses on live-cell imaging systems and confocal microscopy.

Supplementary materials

Supplementary material associated with this article can be found, in the online version, at doi:10.1016/j.bbiosy.2022.100045.

References

[1] Dorrance AM, Neviani P, Ferenchak GJ, Huang X, Nicolet D, Maharry KS, Ozer HG, Hoellarbauer P, Khalife J, Hill EB, Yadav M, Bolon BN, Lee RJ, Lee LJ, Croce CM, Garzon R, Caligiuri MA, Bloomfield CD, Marcucci G. Targeting leukemia stem cells in vivo with antagomiR-126 nanoparticles in acute myeloid leukemia. Leukemia 2015;29:2143–53 https://doi.org/10.1038/leu.2015.139.
[2] Trujillo-Alonso V, Pratt EC, Zong H, Lara-Martinez A, Kaittanis C, Rabie MO, Longo V, Becker MW, Roboz GJ, Grimm J, Guzman ML. FDA-approved ferumoxytol displays anti-leukaemia efficacy against cells with low ferroportin levels. Nat Nanotechnol 2019;14:616–22 https://doi:10.1038/s41565-019-0406-1.
[3] Zhu J, Emerson SG. A new bone to pick: osteoblasts and the haematopoietic stem-cell niche. Bioessays 2004;26:595–9 https://doi:10.1002/bies.20052.
[4] Taichman RS. Blood and bone: two tissues whose fates are intertwined to create the hematopoietic stem-cell niche. Blood 2005;105:2631–9 https://doi:10.1182/blood-2004-06-2480.
[5] Levesque JP, Winkler IG. Cell Adhesion Molecules in Normal and Malignant Hematopoiesis: from Bench to Bedside. Curr Stem Cell Rep 2016;2:356–67 https://doi.org/10.1007/s40778-016-0066-0.
[6] Shah J, Guerrera D, Vasileva E, Sluysmans S, Bertels E, S Citi. PLEKHA7: cytoskeletal adaptor protein at center stage in junctional organization and signaling. Int J Biochem Cell Biol 2016;75:112–16 https://doi:10.1016/j.biocel.2016.04.001.
[7] Takeich M. Dynamic contacts: rearranging adherens junctions to drive epithelial remodelling. Nat Rev Mol Cell Biol 2014;15:397–410 https://doi:10.1038/nrm3802.
[8] Harris TJ, Tepass U. Adherens junctions: from molecules to morphogenesis. Nat Rev Mol Cell Biol 2010;11:502–14 https://doi:10.1038/nrm2927.
[9] Kurita S, Yamada T, Rikitsu E, Ikeda W, Takai Y. Binding between the junctional proteins afadin and PLEKHA7 and implication in the formation of adherens junction in epithelial cells. J Biol Chem 2013;288:29356–68 https://doi:10.1074/jbc.M113.453464.
[10] Citi S, Pulimeno P, Paschoud S. Cingulin, paracingulin, and PLEKHA7: signaling and cytoskeletal adaptors at the apical junctional complex. Ann N Y Acad Sci 2012;1257:125–32 https://doi:10.1111/j.1749-6632.2012.06506.x.
[11] Tille JC, Ho L, Shah J, Seyde O, McKee TA, Citi S. The expression of the zonula adhaerens protein PLEKHA7 is strongly decreased in high grade ductal and lobular breast carcinomas. PLoS ONE 2015;10:e0135442 https://doi:10.1371/journal.pone.0135442.
[12] Pence LJ, Kourtidis A, Feathers RW, Haddad MT, Sotiriou S, Decker PA, Nassar A, Ocal IT, Shah SS, Anastasiadis PZ. PLEKHA7, an apical adherens junction protein, suppresses inflammatory breast cancer in the context of high E-Cadherin and p120-catenin expression. Int J Mol Sci 2021;22:1275 https://doi:10.3390/ijms22031275.
[13] Rea K, Roggiani F, De Cecco L, Raspagliesi F, Carcangiu ML, Nair-Menon J, Bagnoli M, Bortolomai I, Mezzanzanica D, Canevari S, Kourtidis A, Anastasiadis PZ, Tomassetti A. Simultaneous E-cadherin and PLEKHA7 expression negatively affects E-cadherin/EGFR mediated ovarian cancer cell growth. J Exp Clin Cancer Res 2018;37:146 https://doi:10.1186/s13046-018-0796-1.
[14] Mendonsa AM, Na TY, Gumbiner BM. E-cadherin in contact inhibition and cancer. Oncogene 2018;37:4769–80 https://doi:10.1038/s41388-018-0304-2.
[15] Kourtidis A, Ngok SP, Pulimeno P, Feathers RW, Carpio LR, Baker TR, Carr JM, Yan IK, Borges S, Perez EA, Storz P, Copland JA, Patel T, Thompson EA, Citi S, Anastasiadis PZ. Distinct E-cadherin-based complexes regulate cell behaviour through miRNA processing or Src and p120 catenin activity. Nat Cell Biol 2015;17:1145–57 https://doi:10.1038/ncb3227.
[16] Meng W, Mushika Y, Ichii T, Takeichi M. Anchorage of microtubule minus ends to adherens junctions regulates epithelial cell-cell contacts. Cell 2008;135:948–59 https://doi:10.1016/j.cell.2008.09.040.
[17] Pulimeno P, Bauer C, Stutz J, Citi S. PLEKHA7 is an adherens junction protein with a tissue distribution and subcellular localization distinct from ZO-1 and E-cadherin. PLoS ONE 2010;5:e12207 https://doi:10.1371/journal.pone.0012207.
[18] Kourtidis A, Anastasiadis PZ. PLEKHA7 defines an apical junctional complex with cytoskeletal associations and miRNA-mediated growth implications. Cell Cycle 2016;15:498–505 https://doi:10.1080/15384101.2016.1141840.
[19] Ladikou EE, Sivaloganathan H, Pepper A, Chevassut T. Acute myeloid leukaemia in its niche: the bone marrow microenvironment in acute myeloid leukaemia. Curr Oncol Rep 2020;22:27 https://doi:10.1007/s11912-020-0885-0.
[20] Yamaguchi T, Kawamoto E, Gaowa A, Park EJ, Shimaoka M. Remodeling of bone marrow niches and roles of exosomes in leukemia. Int J Mol Sci 2021;22:1881 https://doi:10.3390/ijms22041881.
[21] Asada N. Regulation of malignant hematopoiesis by bone marrow microenvironment. Front Oncol 2018;8:119 https://doi:10.3389/fonc.2018.00119.
[22] Yetisgin AA, Cetinel S, Zuvin M, Kosar A, Kutlu O. Therapeutic nanoparticles and their targeted delivery applications. Molecules 2020;25:2193 https://doi:10.3390/molecules25092193.
[23] Hallan SS, Sguizzato M, Esposito E, Cortesi R. Challenges in the physical characterization of lipid nanoparticles. Pharmaceutics 2021;13:549 https://doi:10.3390/pharmaceutics13040549.
[24] Matei AM, Caruntu C, Tampa M, Georgescu SR, Matei C, Constantin MM, et al. Applications of nanosized-lipid-based drug delivery systems in wound care. Appl Sci 2021;11(11):4915 https://doi.org/10.3390/app11114915.
[25] Pelaz B, del Pino P, Maffre P, Hartmann R, Gallego M, Rivera-Fernández S, de la Fuente JM, Nienhaus GU, Parak WJ. Surface functionalization of nanoparticles with polyethylene glycol: effects on protein adsorption and cellular uptake. ACS Nano 2015;9:6996–7008 https://doi:10.1021/acsnano.5b01326.

[26] Suk JS, Xu Q, Kim N, Hanes J, Ensign LM. PEGylation as a strategy for improving nanoparticle-based drug and gene delivery. Adv Drug Deliv Rev 2016;99:28–51 https://doi:10.1016/j.addr.2015.09.012.
[27] Fam SY, Chee CF, Yong CY, Ho KL, Mariatulqabtiah AR, Tan WS. Stealth coating of nanoparticles in drug-delivery systems. Nanomaterials 2020;10:787 https://doi:10.3390/nano10040787.
[28] Termsarasab U, Yoon IS, Park JH, Moon HT, Cho HJ, Kim DD. Polyethylene glycol-modified arachidyl chitosan-based nanoparticles for prolonged blood circulation of doxorubicin. Int J Pharm 2014;464:127–34 https://doi:10.1016/j.ijpharm.2014.01.015.
[29] Hoang Thi TT, Pilkington EH, Nguyen DH, Lee JS, Park KD, Truong NP. The importance of poly(ethylene glycol) alternatives for overcoming PEG immunogenicity in drug delivery and bioconjugation. Polymers (Basel) 2020;12:298 https://doi:10.3390/polym12020298.
[30] Zhao J, Santino F, Giacomini D, Gentilucci L. Integrin-targeting peptides for the design of functional cell-responsive biomaterials. Biomedicines 2020;8:307 https://doi:10.3390/biomedicines8090307.
[31] Danhier F, Breton ALe, Préat V. RGD-based strategies to target alpha(v) beta(3) integrin in cancer therapy and diagnosis. Mol Pharm 2012;9:2961–73 https://doi:10.1021/mp3002733.
[32] Rios De La Rosa JM, Spadea A, R Donno, Lallana E, Lu Y, Puri S, Caswell P, Lawrence MJ, Ashford M, Tirelli N. Microfluidic-assisted preparation of RGD-decorated nanoparticles: exploring integrin-facilitated uptake in cancer cell lines. Sci Rep 2020;10:14505 https://doi:10.1038/s41598-020-71396-x.
[33] Rouaud F, Sluysmans S, Flinois A, Shah J, Vasileva E, Citi S. Scaffolding proteins of vertebrate apical junctions: structure, functions and biophysics. Biochim Biophys Acta Biomembr 2020;1862:183399 https://doi:10.1016/j.bbamem.2020.183399.
[34] Kourtidis A, Necela B, Lin WH, Lu R, Feathers RW, Asmann YW, Thompson EA, Anastasiadis PZ. Cadherin complexes recruit mRNAs and RISC to regulate epithelial cell signaling. J Cell Biol 2017;216:3073–85 https://doi:10.1083/jcb.201612125.
[35] Yang J, Bahreman A, Daudey G, Bussmann J, Olsthoorn RC, Kros A. Drug delivery via cell membrane fusion using lipopeptide modified liposomes. ACS Cent Sci 2016;2:621–30 https://doi:10.1021/acscentsci.6b00172.
[36] Zhang L, Yang X, Lv Y, Xin X, Qin C, Han X, Yang L, He W, Yin L. Cytosolic co-delivery of miRNA-34a and docetaxel with core-shell nanocarriers via caveolae-mediated pathway for the treatment of metastatic breast cancer. Sci Rep 2017;7:46186 https://doi:10.1038/srep46186.
[37] Nair-Menon J, Daulagala AC, Connor DM, Rutledge L, Penix T, Bridges MC, Wellslager B, Spyropoulos DD, Timmers CD, Broome AM, Kourtidis A. Predominant distribution of the RNAi machinery at apical adherens junctions in colonic epithelia is disrupted in cancer. Int J Mol Sci 2020;21:2559 https://doi:10.3390/ijms21072559.
[38] Rao Q, Wang JY, Meng J, Tang K, Wang Y, Wang M, Xing H, Tian Z, Wang J. Low-expression of E-cadherin in leukaemia cells causes loss of homophilic adhesion and promotes cell growth. Cell Biol Int 2011;35:945–51 https://doi:10.1042/CBI20100456.
[39] Rao Q, Xu ZF, Wang JY, Meng JH, Tang KJ, Tian Z, Xing HY, Wang M, Wang JX. Leukemia cell surface expression of E-cadherin and its correlation with membrane localization of beta-catenin. Zhonghua Xue Ye Xue Za Zhi (in Chinese) 2008;29:592–4 PMID: 19175984.
[40] Wang B, Li X, Liu L, Wang M. β-Catenin: oncogenic role and therapeutic target in cervical cancer. Biol Res 2020;53:33 https://doi:10.1186/s40659-020-00301-7.
[41] Azbazdar Y, Karabicici M, Erdal E, Ozhan G. Regulation of Wnt signaling pathways at the plasma membrane and their misregulation in cancer. Front Cell Dev Biol 2021;9:631623 https://doi:10.3389/fcell.2021.631623.
[42] Kaplan RN, Psaila B, Lyden D. Niche-to-niche migration of bone-marrow-derived cells. Trends Mol Med 2007;13:72–81 https://doi:10.1016/j.molmed.2006.12.003.
[43] Zhang P, Zhang C, Li J, Han J, Liu X, Yang H. The physical microenvironment of hematopoietic stem cells and its emerging roles in engineering applications. Stem Cell Res Ther 2019;10:327 https://doi:10.1186/s13287-019-1422-7.
[44] Kulkarni R, Kale V. Physiological cues involved in the regulation of adhesion mechanisms in hematopoietic stem cell fate decision. Front Cell Dev Biol 2020;8:611 https://doi:10.3389/fcell.2020.00611.
[45] Chen S, Lewallen M, Xie T. Adhesion in the stem cell niche: biological roles and regulation. Development 2013;140:255–65 https://doi:10.1242/dev.083139.
[46] Zhou J, Mauerer K, Farina L, Gribben JG. The role of the tumor microenvironment in hematological malignancies and implication for therapy. Front Biosci 2005;10:1581–96 https://doi:10.2741/1642.